Front. Chem. Sci. Eng. 2024, 18(1): 2
https://doi.org/10.1007/s11705-023-2368-y

RESEARCH ARTICLE

Electrochemical anodization of cast titanium alloys in oxalic acid for biomedical applications

Engie M. Safwat[1], Soha A. Abdel-Gawad (✉)[2], Madiha A. Shoeib[3], Shimaa El-Hadad[3]

1 Restorative and Dental Materials Department, National Research Centre, Giza 12622, Egypt
2 Chemistry Department, Faculty of Science, Cairo University, Giza 12613, Egypt
3 Central Metallurgical Research and Development Institute, Helwan 11421, Egypt

Abstract Titanium and its alloys have numerous biomedical applications thanks to the composition and morphology of their oxide film. In this study, the colorful oxide films were formed by anodizing cast Ti-6Al-4V and Ti-6Al-7Nb alloys in a 10% oxalic acid solution for 30 s at different voltages (20–80 V) of a direct current power supply. Atomic force microscopy was used as an accurate tool to measure the surface roughness of thin films on the nanometer scale. Scanning electron microscopy and X-ray diffraction were performed to analyze surface morphology and phase structure. According to the results, the produced titanium oxide layer showed high surface roughness, which increased with increasing anodizing voltage. The impact of anodizing voltages on the color and roughness of anodized layers was surveyed. The corrosion resistance of the anodized samples was studied in simulated body fluid at pH 7.4 and a temperature of 37 °C utilizing electrochemical impedance spectroscopy and the potentiodynamic polarization method. The anodized samples for both alloys at 40 V were at the optimal voltage, leading to a TiO_2 layer formation with the best compromise between oxide thickness and corrosion resistance. Also, findings showed that TiO_2 films produced on Ti-6Al-7Nb alloys had superior surface roughness properties compared to those of Ti-6Al-4V alloys, making them more appropriate for orthopedic applications. From the obtained data and the fruitful discussion, it was found that the utilized procedure is simple, low-cost, and repeatable. Therefore, anodization in 10% oxalic acid proved a viable alternative for the surface finishing of titanium alloys for biomedical applications.

Keywords DC anodization, Ti-6Al-4V alloy, Ti-6Al-7Nb alloy, oxide film, corrosion

Received June 19, 2023; accepted August 21, 2023;
online November 7, 2023

E-mails: Soha.gawad@cu.edu.eg, Soha.gawad@yahoo.com

1 Introduction

Titanium and its alloys are utilized extensively in various industries due to their unique traits, such as their low modulus of elasticity, elevated strength-to-weight ratio, great biocompatibility, and corrosion resistance [1]. Titanium alloys are popular as implant materials for orthopedic and dental applications due to their favorable mechanical properties and biocompatibility [2,3]. Surface properties like chemical composition and topography influence this biocompatibility. The naturally formed TiO_2 layer in the initial stages of the osseointegration process is not optimal for bone adhesion and growth [4,5]. Furthermore, post-surgical problems include implant-associated infection and mechanical loosening, compromising long-term performance. Ti-6Al-4V is the most commonly utilized $\alpha + \beta$ Ti alloy and is frequently employed for surgical repair and replacement implants, such as intramedullary nails, hip joints, dental implants, and bone plates [6,7]. However, the release of V and Al ions, which have toxic effects and result in various health problems over time, such as systemic dermatitis, peripheral neuropathy, and Alzheimer's, makes long-term implantation of Ti-6Al-4V raise safety concerns [8,9]. Then, researchers created V-free Ti alloys such as Ti-6Al-7Nb, which had mechanical and metallurgical characteristics almost similar to Ti-6Al-4V [10]. Despite the effectiveness of V-free Ti alloys, the Al content of the materials might contribute to various osteal and neural issues. As a result of the aforementioned defects, surface modification can be used to overcome these problems while keeping the required bulk properties [11].

Anodization is an electrochemical surface modification process applied on metallic surfaces to alter oxide layer thickness, composition, and morphology [12,13]. It is a low-cost, one-step method that involves applying a constant voltage or current between the working and

counter electrodes of an electrochemical cell. This causes metal atoms, particularly those of titanium and its alloys, to oxidize to Ti^{4+} ions that bond with oxide anions from the electrolyte, thus gradually yielding an oxide layer on the metal surface [14]. Based on the properties of the oxide that forms, titanium and its alloys can be anodized in three ways: the first way is the traditional anodization, producing compact, thin, and colored films; the second way is the anodization in fluoride-containing electrolytes, producing nanotubular oxides, and the third way is the high voltage anodization, known as plasma electrolytic oxidation or micro-arc oxidation [15,16].

Titanium anodizing is performed in acid and salt solutions. Usually, oxalic acid ($C_2H_2O_4$), a strong acid, can be used as an anodizing electrolyte in concentrations of 3% up to 10% [17], producing an interference-colored oxide film on titanium [18,19]. The surface color of titanium varies with the oxide thickness, which depends on the applied voltage and electrolyte type. Oxalic acid plays a specific role in the anodizing process of medical implants; apart from forming a barrier layer in the biological environment, it also provides a desirable porous surface that supports implant fixation and bone growth into open pore spaces, thereby improving the bone-implant interface and avoiding implantation failure [20,21]. A TiO_2 layer typically has oxygen vacancies in the lattice of the TiO_2 crystal, and these serve as important sites for the adsorption and stimulation of numerous surface processes. Particularly, H_2O dissociation causes the production of two OH groups on the surface [22]. These OH groups enhance the uptake of Ca^{2+} ions and encourage the hydroxyapatite ($Ca_{10}(PO_4)_6(OH)_2$) creation, which are essential elements in the coating development. Hydroxyapatite, is a ceramic biomaterial, enhances bone integration with the implant. However, the process of anodizing titanium alloys with oxalic acid still needs to be fully understood and requires additional research.

This study compared thin oxide films grown on Ti-6Al-4V and Ti-6Al-7Nb alloys by anodization in a 10% oxalic acid solution for 30 s at 0–80 V of a direct current (DC) power supply. This research aims to provide a suitable surface and enhance the titanium alloy's lifetime (corrosion rate) as a biomedical implant inside the human body. The tested alloys' surface topography and morphological characteristics were characterized using atomic force microscopy (AFM). The corrosion behavior of alloys was investigated in simulated body fluid (SBF).

2 Experimental

2.1 Fabrication of titanium alloy specimens

The investigation specimens used in the current study were prepared by remelting pieces of Ti-6Al-4V and Ti-6Al-7Nb alloys (provided by Baoji Xuhe Titanium Metal Co., Ltd.) in a vacuum arc furnace (model LHD 1250). The process starts by inserting pieces of each alloy in the melting chamber inside a copper-cooled mold, as shown in Fig. 1. This was followed by evacuating the melting chamber to avoid titanium reactivity and ensure a clean melting process. When the required vacuum level was reached, a high voltage was applied between the tungsten electrode and the copper mold. This resulted in an arc initiation, which melted the charge inside the mold. To guarantee homogeneity, electromagnetic stirring was used, and the samples were remelted several times until sound rod samples were obtained. The figure shows the melting process and the mold wherein the charge was inserted. The obtained rods were then finished using a turning machine and cut into 80 mm diameter and 10 mm high discs. The chemical composition of the samples was analyzed by an inductively coupled plasma atomic-emission spectroscopy method, as shown below in Table 1.

2.2 Preparation of the samples

The Ti alloy discs were fixed in an epoxy resin block, exposing an area of 0.5 cm^2. When immersed in an electrolyte solution, a teflon-coated stainless-steel rod held each disc in place. The discs were mechanically polished with SiC sheets up to 2400 grit and then cleaned ultrasonically in deionized water for 5 min. The Ti alloy discs were etched in a mixture of 80 $mL \cdot L^{-1}$ HNO_3,

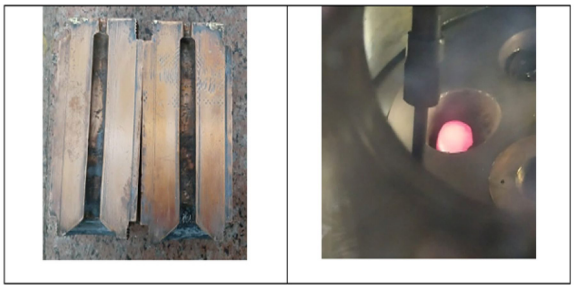

Fig. 1 The copper mold used for preparing the rod-shaped samples and the molten charge inside the vacuum chamber of the arc furnace.

Table 1 Chemical composition of Ti-6Al-4V and Ti-6Al-7Nb alloys

Element	Al	Nb	V	Ta	Fe	C	O	N	Others	Ti
Ti-6Al-4V	6.1	0.01	4.00	0	0.10	0.02	0.03	0.01	< 0.4	Bal.
Ti-6Al-7Nb	6.2	6.80	0.01	< 0.05	0.03	< 0.01	0.14	< 0.01	< 0.4	Bal.

60 mL·L^{-1} HF, and 150 mL·L^{-1} H_2O_2 for 2 min at room temperature. After ultrasonic cleaning, the samples were in deionized water for 5 min and air-dried.

2.3 Anodization of the samples

A DC power supply was utilized to power the anodization process potentiostatically in a 10% oxalic acid solution for 30 s at room temperature in the voltage range of 20–80 V. The designed electrochemical cell has two electrodes: a cathode made of the platinum basket and an anode made of a sample of Ti alloy. The cathode and anode were separated by about 4 cm.

2.4 Surface characterization

Macrographs taken by a stereoscope were used to measure the average grain. Optical micrographs were not ideal for calculations since the grain size was large enough to be seen by the naked eye. The grain size was measured using the linear intercept method [23], where random straight lines were drawn on the micrograph. The length of each line (considering the magnification) was then divided by the number of intersections. Finally, the average of all the lines was considered and repeated for several micrographs.

The surface roughness and morphology of the tested samples were inspected using an AFM (Anton Paar-Tosca™ 200, USA). After anodization, images were recorded at randomly selected locations. A scanning size of 10 μm × 10 μm with a resolution of 400 × 400 was acquired using an arrow NCR tapping cantilever. To evaluate the surface roughness, the AFM data were processed according to ISO 25178 using Tosca analysis software, a specialized program. Scanning electron microscope (SEM, JEOL-JSM-5410, Japan) was used to determine the oxide film thickness on anodized Ti alloy by preparing a cross-section of selected samples. X-ray diffraction (XRD) thin film, model "BRUKER-D8 DISCOVER" operated at 40 kV and 40 mA, with a CuKα radiation; (λ = 0.154 nm) was used for identifying the surface constituting elements/compounds after anodization.

2.5 Electrochemical test

Electrochemical measurements were performed at 37 °C utilizing a potentiostat/galvanostat (Auto Laboratory PGSTAT 302N, Netherlands) in SBF solution containing (g·L^{-1}(NaCl 8, $CaCl_2$ 0.14, KCl 0.4, $NaHCO_3$ 0.35, $C_6H_{12}O_6$ 1, NaH_2PO_4 0.1, $MgCl_2 \cdot 6H_2O$ 0.1, $Na_2HPO_4 \cdot 2H_2O$ 0.06, and $MgSO_4 \cdot 7H_2O$ 0.06 at pH 7.4 [24,25]. A three-electrode cell with 100 mL SBF was used, with Ag/AgCl as the reference electrode, platinum as the counter electrode, and titanium or anodized titanium alloys as the working electrodes. The potentiodynamic studies started once the open-circuit potentials had stabilized for 30 min. A perturbation amplitude of 5 mV was used for electrochemical impedance spectroscopy (EIS) in the frequency range of 10 MHz–100 kHz. Potentiodynamic polarization curves between –0.8 and 1.0 V were measured at a scan rate of 1 mV·s^{-1}.

3 Results and discussion

3.1 Microstructure of the prepared samples

Figure 2 displays the microstructure of the as-cast samples. As known for the cast microstructure of the two-phase titanium alloys, it comprises Widmanstädten α with prior β grains. It is remarkable here that the grain size of the Ti-6Al-7Nb specimen, shown in Fig. 2(b), is finer than that of Ti-6Al-4V presented in Fig. 2(a). According to the grain size measurements, the average grain size for Ti-6Al-4V was calculated to be ca. 4.6 mm, while for Ti-6Al-7Nb, it was ca. 3.2 mm. An example of the macrographs used for calculations is shown in Fig. 2. The differences in the original microstructure and the beta phase stabilizing elements (V and Nb) between the two alloys are expected to influence their response to the anodization. It was previously reported that these two alloys responded differently upon surface modification using oxidation [26,27].

3.2 Anodization process

The anodization of Ti-6Al-4V and Ti-6Al-7Nb was done in 10% oxalic acid for 30 s at different voltages from 20 to 80 V of a DC power supply. The oxide films were successfully formed, and the different anodizing voltages provided different colors, as shown in Table 2. The polished Ti alloy without anodization displays a brilliant metallic shine. After anodization, it is generally acknowledged that the colors seen are caused by the light interference phenomenon of reflected light between the oxide film surfaces [28]. As light rays fell on an anodized surface, owing to the different pores on the oxide layer, light reflection took place at different angles; thus, diverse, scattered images were created for each oxide layer with various surface colors [29].

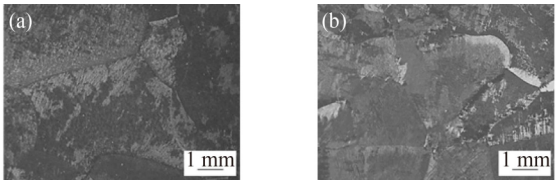

Fig. 2 Stereo macrographs of (a) Ti-6Al-4V and (b) Ti-6Al-7Nb as-cast alloys.

Table 2 Color of oxide films produced on the Ti-6Al-4V and Ti-6Al-7Nb alloys in the presence of 10% oxalic acid for 30 s at different DC voltages (0–80 V)

Voltage	Ti-6Al-4V		Ti-6Al-7Nb	
	Color	Image	Color	Image
0 V	Silvery		Silvery	
20 V	Blue		Crimson	
40 V	Light green		Green	
60 V	Dark yellow		Dark yellow	
80 V	Dark blue with purple spots		Dark blue with purple spots	

3.3 Surface roughness

AFM photographs were taken to examine the surface morphology and roughness of the oxide film produced on Ti-6Al-4V and Ti-6Al-7Nb alloy surfaces at different voltages. These characteristics are crucial because they affect the materials' biocompatibility and corrosion behavior. Also, surface features impact the functional activity of cells interacting with biomaterials. The three-dimensional and cross-sectional profiles of Ti-6Al-4V and Ti-6Al-7Nb oxidized surfaces are displayed in Figs. 3 and 4, respectively. These images reveal that each sample has a different morphology, and the surface at 0 V (before anodization) is almost smooth and homogeneous, with an average surface roughness S_a (94 and 127 nm) and a root mean square S_q (112 and 153 nm) for Ti-6Al-4V and Ti-6Al-7Nb, respectively. The formation of the oxide layer during anodization was uneven, and the presence of defects increased roughness. Moreover, as the anodizing voltage increases, the roughness of the oxide films produced on both alloys continues to increase until they reach a maximum value at 80 V. Others have reported comparable results [30–32]. Table 3 presents S_a and S_q values obtained from AFM. Rough surfaces increase the accessible surface area for cell adhesion, which may undergo osteoblast differentiation to form a bone matrix. Successful osseointegration improves clinical results [33,34]. According to the results, the surface roughness of anodized Ti-6Al-7Nb is greater than that of anodized Ti-6Al-4V, making them more suitable for orthopedic applications since rough surfaces facilitate implant osseointegration.

Typical line profiles from section analysis were generated for anodized Ti-6Al-4V and Ti-6Al-7Nb surfaces and presented in Figs. 3 and 4. The heights of the peaks in line profiles for anodizing Ti-6Al-4V and Ti-6Al-7Nb increased with an increase in anodizing voltage. The pronounced elevations in the size of the peaks indicated that the TiO_2 films' thickness increased with anodization voltages. The average thickness of the oxide layer depends on the applied voltage and increases with increasing voltages from 0 to 80 V [35,36]. The results of the line profile confirm much rougher properties of anodized Ti-6Al-7Nb, which is consistent with the AFM topography images.

SEM analyzed the average thickness of the oxide layer (TiO_2). Figures 5 and 6 present SEM images of cross sections for Ti-6Al-4V and Ti-6Al-7Nb alloy subjected to anodization in 10% oxalic acid for 30 s at anodization voltages of 20 and 80 V. The anodizing process is expected to form a continuous oxide layer with thickness increases with the applied voltage. A general view of the oxide layer on Ti-6Al-4V alloy in 10% oxalic acid for 30 s at anodization voltages of 20 and 80 V is shown in Figs. 5(a) and 5(c). It was apparent that there was a significant difference between the thickness of the oxide layer developed at different voltages. Figure 5(b) presented the thickness of TiO_2 at anodization 20 V ranging between ca. 5–6.9 μm, and that formed at 80 V was formed between ca. 14.3–14.8 μm as represented in Fig. 5(d).

Figures 6(a) and 6(c) shows a general outlook of the oxide layer on Ti-6Al-7Nb alloy anodized at voltages 20 and 80 V. Figure 6(b) revealed that the thickness of the oxide layer developed on the surface of Ti-6Al-7Nb alloy anodized at 20 V ranged between ca. 7.4–9.8 μm. Figure 6(d) showed that the thickness of the oxide layer at anodized voltage 80 V was found in the range of ca. 19–20.8 μm, confirming that increasing voltage greatly enhanced the formation of TiO_2. These results confirm the outcomes of this study, the Ti-6Al-7Nb alloy is the most adequate alloy with excellent osteointegration properties.

Generally, anodization is a conventional electrochemical method to generate a protecting dense barrier-type oxide coating on Ti alloys. During anodization, the oxidized metal species Ti^{4+} generated at the metal/oxide interface (Eq. (1)) moves outward. In contrast oxygen ions O^{2-} formed by the deprotonation of H_2O (Eq. (2)) at the oxide/electrolyte interface moves inward. Thus, according to Eq. (3), compact titanium oxide is formed at both interfaces through this field-assisted ion migration. During anodization, the oxide film thickens if the electric field is powerful enough to provoke ionic conduction across the oxide.

$$Ti \rightarrow Ti^{4+} + 4e^{-} \quad (1)$$

$$H_2O \rightarrow O^{2-} + 2H^{+} \quad (2)$$

$$Ti^{4+} + 2O^{2-} \rightarrow TiO_2 \quad (3)$$

where the overall reaction is

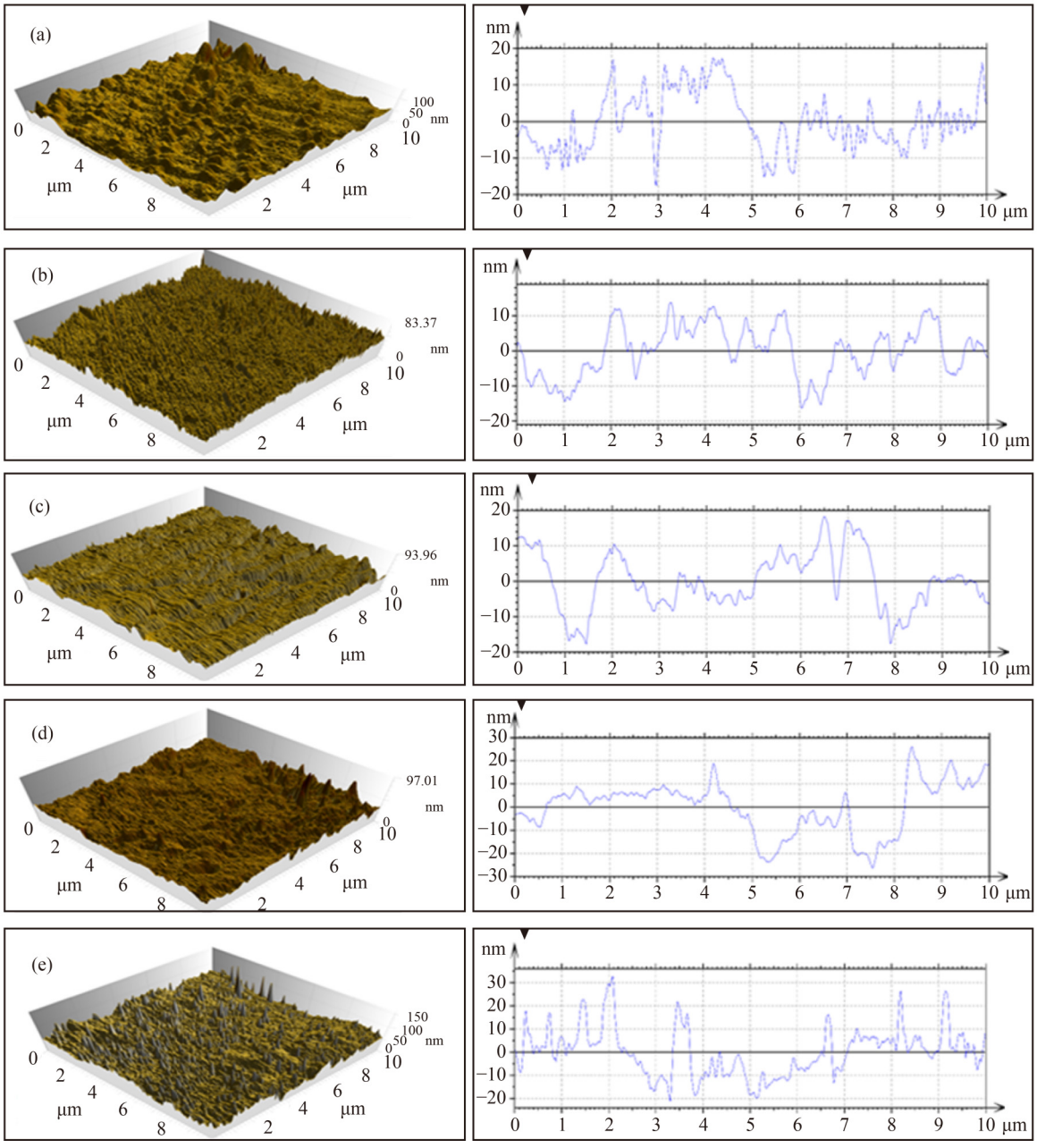

Fig. 3 Three-dimensional images and cross-sectional profiles of anodic oxide films on Ti-6Al-4V alloy in 10% oxalic acid for 30 s at anodization voltages of (a) 0, (b) 20, (c) 40, (d) 60, and (e) 80 V.

$$Ti + 2H_2O \rightarrow TiO_2 + 4H^+ + 4e^- \quad (4)$$

The total reaction forms a stable oxide film, TiO_2, and its growth is enhanced by increasing the applied voltage (0–80V). This film provides an efficient corrosion and leakage barrier against toxic ions, increasing biocompatibility [5,37,38].

Figures S1 and S2 (cf. Electronic Supplementary Material) depict two-dimensional images of bare and anodized Ti-6Al-4V and Ti-6Al-7Nb alloys. Bare alloys, Ti-6Al-4V and Ti-6Al-7Nb in Figs. S1(a) and S2(a), exhibit homogeneous and uniform surfaces. Figures S1(b–e) and S2(b–e) show that compact TiO_2 growth is proportional to an applied voltage and affects roughness. High voltages promote the inward transfer of O^{2-} into the metal film interface and the diffusion of Ti^{4+} ions from the titanium alloys to the electrolyte interface at the anode, which thickens the oxide film.

The chemical phase composition of the TiO_2 layer was confirmed by XRD analysis. Figure 7 shows the XRD patterns of the Ti-6Al-4V and Ti-6Al-7Nb alloy after anodization at 40 V, respectively (optimal condition). All the samples show that the oxide layer mainly consists of the anatase TiO_2 phase with peaks appearing at main diffraction peaks observed at $2\theta = 38.2°$, 53.5°, and 62.2° for both alloys. These results were in good agreement with JCPDS Card No. 21-1272. Moreover, the 40.3° and

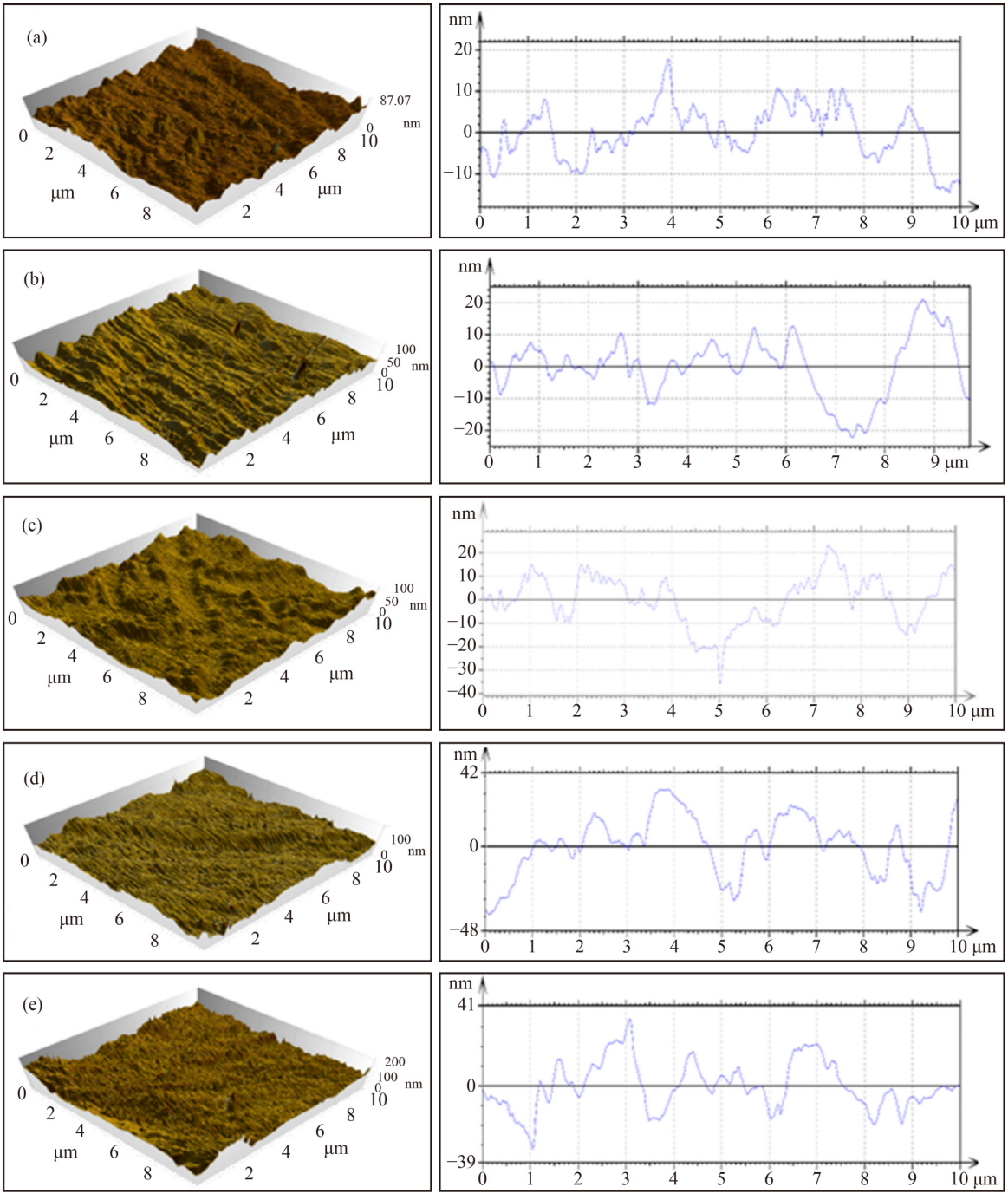

Fig. 4 Three-dimensional images and cross-sectional profiles of anodic oxide films on Ti-6Al-7Nb alloy in 10% oxalic acid for 30 s at anodization voltages of (a) 0, (b) 20, (c) 40, (d) 60, and (e) 80 V.

70.7° peaks are attributed to titanium substrate with standard JCPDS Card No. 44-1294.

3.4 Electrochemical analysis

Electrochemical studies in SBF solution at 37 °C were carried out to establish whether the produced oxides give corrosion protection to the substrate. Figure 8 present the potentiodynamic polarization curves of Ti-6Al-4V and Ti-6Al-7Nb alloys anodized in 10% oxalic acid for 30 s.

Table 3 S_a and S_q for anodized Ti-6Al-4V and Ti-6Al-7Nb alloy surface at different voltages (0–80 V)

Applied DC voltage	Ti-6Al-4V		Ti-6Al-7Nb	
	S_a/nm	S_q/nm	S_a/nm	S_q/nm
0 V	94	112	127	153
20 V	108	128	131	155
40 V	154	181	196	234
60 V	188	208	228	264
80 V	324	397	388	481

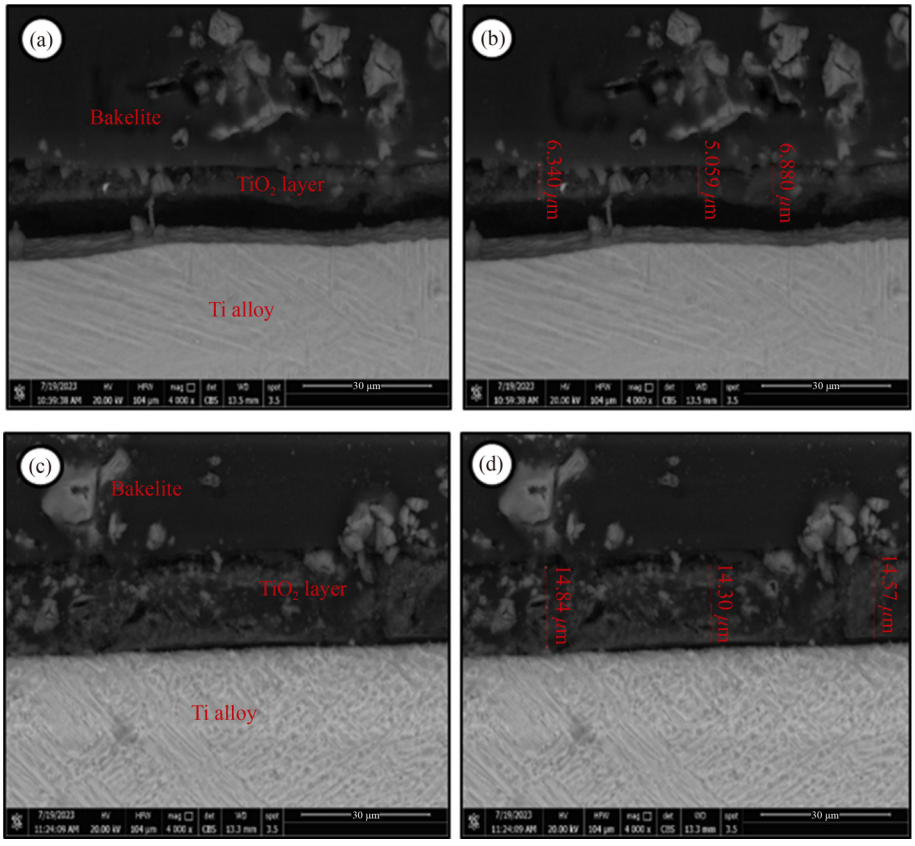

Fig. 5 SEM image of cross-sections of TiO_2 layer on Ti-6Al-4V alloy in 10% oxalic acid for 30 s at anodization voltages of (a, b) 20 and (c, d) 80 V.

According to the polarization diagrams, anodization improves surface resistance for both alloys via shifting the corrosion potential in a noble (positive) direction and decreasing corrosion current density compared to non-anodized titanium samples. The results suggest that anodization can protect titanium alloys and increase their corrosion resistance in SBF. The anodic film was a barrier to block the solution from penetrating the metal surface [39]. The optimal anodization voltage for both alloys is 40 V with stable TiO_2 film. However, Ti-6Al-7Nb showed lower corrosion current densities than Ti-6Al-4V, demonstrating a more stable oxide film for the Ti-6Al-7Nb alloy.

The improved oxide film development and better corrosion performance of the alloy Ti-6Al-7Nb could be ascribed to the Nb presence. A previous study reported the positive effects of adding Nb to Ti-based alloys on surface film stabilization [40]. Moreover, Nb cations lower the anion vacancy concentration on the titanium oxide film, improving surface film passivation. Lower titanium oxidation states produce anions [41,42]. Therefore, the existence of Nb in the passive film of Ti-6Al-7Nb may be the reason for its low corrosion current density compared to Ti-6Al-4V [43].

Using Tafel slopes, the Stern-Geary equation shows that the polarization resistance is related to the corrosion current [44,45]:

$$R_p = \frac{\beta_a \beta_c}{2.3 \times i_{corr} (\beta_a + \beta_c)}, \quad (5)$$

where β_a and β_c are the anodic and cathodic Tafel slopes.The corrosion current density (i_{corr}) is proportional to the corrosion rate (R_i), as shown in Eq. (6):

$$R_i = K i_{corr} (eq.wt)/d, \quad (6)$$

where R_i is given in $mm \cdot yr^{-1}$, i_{corr} in $\mu A \cdot cm^{-2}$, $K = 3.27 \times 10^{-3}$ $mm \cdot g \cdot \mu A^{-1} \cdot cm^{-1} \cdot yr^{-1}$, *eq.wt* is the equivalent weight for Ti under oxidizing condition, and *d* is the alloy density, 4.5 $g \cdot cm^{-3}$. Equation (7) was used to calculate the corrosion protection efficiency (PE, %) of anodized titanium alloys immersed in SBF solutions at 37 °C [44–46]:

$$PE = 1 - \frac{i_{corr}}{i_{corr^\circ}} \times 100\%, \quad (7)$$

where i_{corr° is the corrosion current densities before anodization, and i_{corr} is the corrosion current densities of the titanium alloy after anodization. The corrosion characteristics presented in the polarization curves, including corrosion potential (E_{corr}), corrosion current density (I_{corr}), polarization resistance (R_p), corrosion rate (R_i), and PE are recorded in Table 4.

Utilizing the EIS technique, the Nyquist plots of anodized Ti-6Al-4V and Ti-6Al-7Nb alloys anodized in 10% oxalic acid for 30 s were examined in a 37 °C SBF

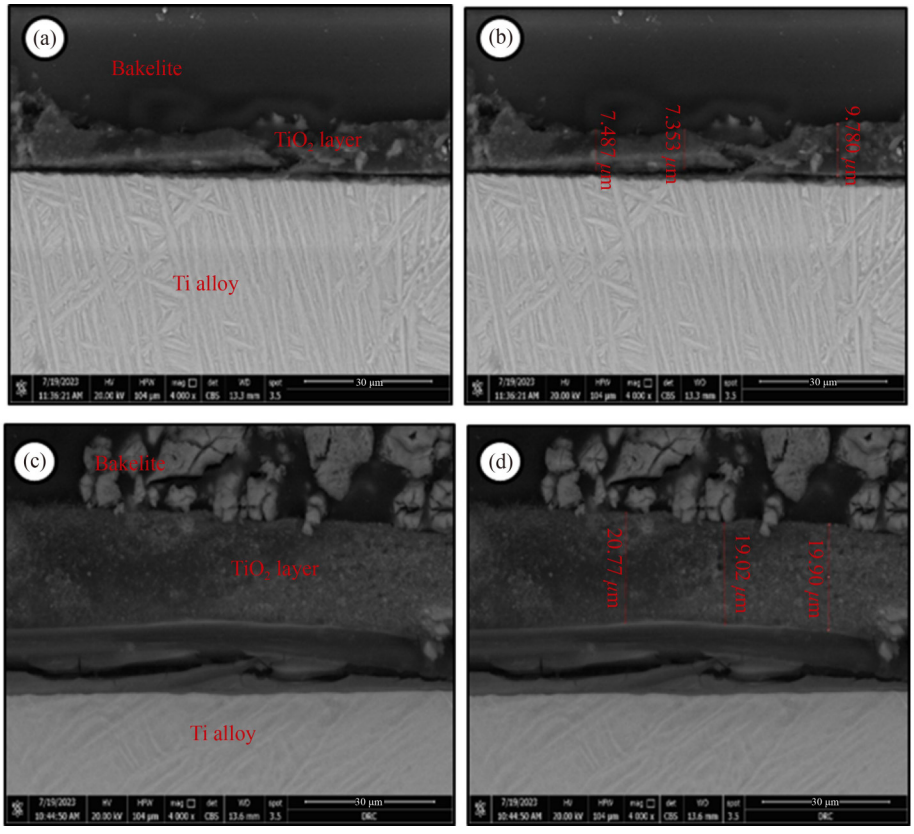

Fig. 6 SEM image of cross-sections of TiO_2 layer on Ti-6Al-7Nb alloy in 10% oxalic acid for 30 s at anodization voltages of (a, b) 20 and (c, d) 80 V.

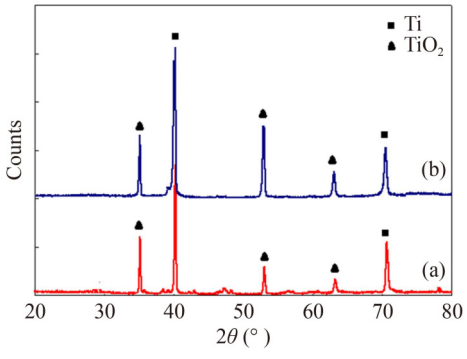

Fig. 7 XRD patterns on the (a) Ti-6Al-4V and (b) Ti-6Al-7Nb alloys anodized at 40 V.

solution. The results are shown in Figs. 9(a) and 9(b) for Ti-6Al-4V and Ti-6Al-7Nb, respectively. The impedance investigation complements the previously obtained polarization data. The Ti-6Al-7Nb showed the best corrosion resistance compared to the Ti-6Al-4V. The electrodes with protective oxide films produced by anodization present superior impedance values compared to the non-anodized; this behavior corresponds to the enhanced corrosion resistance of the uniform, compact passive films. The most stable oxide films were obtained at an applied voltage of 40 V; these results agree with the AFM, where an increase in the applied voltage over 40 V

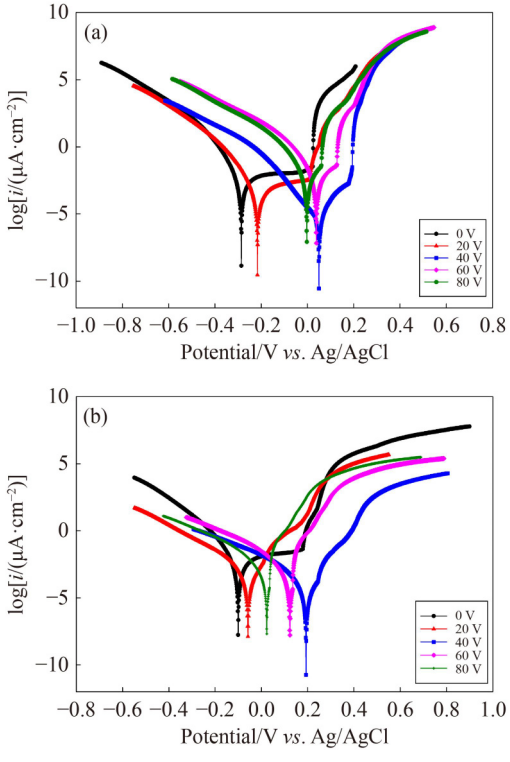

Fig. 8 Potentiodynamic polarization curves of anodized (a) Ti-6Al-4V and (b) Ti-6Al-7Nb in 37 °C SBF solution.

Table 4 Electrochemical parameters and corrosion rates obtained by polarization tests

	Specimens	E_{corr}/V	I_{corr}/(μA·cm^{-2})	R_p/kΩ	R_i/(mm·yr^{-1})	PE/%
Ti-6Al-7Nb	0 V	–0.098	1.9×10^{-3}	8.6	6.9×10^{-4}	–
	20 V	–0.059	1.5×10^{-4}	65.0	5.4×10^{-4}	92.1
	40 V	0.190	6.3×10^{-6}	94.0	2.2×10^{-5}	99.6
	60 V	0.120	3.1×10^{-4}	29.0	7.2×10^{-4}	83.7
	80 V	0.021	5.1×10^{-4}	22.0	9.3×10^{-4}	73.7
Ti-6Al-4V	0 V	–0.294	2.5×10^{-3}	6.4	8.7×10^{-4}	–
	20 V	–0.220	3.1×10^{-4}	56.0	7.2×10^{-4}	87.6
	40 V	0.046	1.5×10^{-5}	89.3	1.1×10^{-4}	99.4
	60 V	0.035	5.2×10^{-4}	27.7	1.9×10^{-4}	79.2
	80 V	–0.024	7.9×10^{-4}	21.2	6.7×10^{-4}	68.4

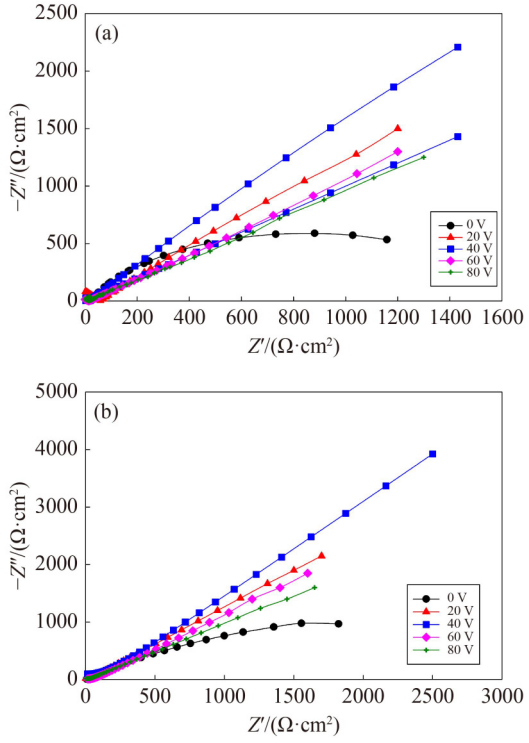

Fig. 9 Nyquist plot curves of anodized (a) Ti-6Al-4V and (b) Ti-6Al-7Nb in 37 °C SBF solution.

increases the roughness, which facilitates cell adhesion and osseointegration of the implant but may increase the metal ion release due to the penetration of the electrolyte, decreasing the corrosion resistance.

The resistance of the passive film of Ti-6Al-4V alloy was less than that of Ti-6Al-7Nb alloy. In the case of Ti-6Al-4V alloy, the vanadium oxide formed on the surface dissolute because of the Cl ions present in the SBF solution. Vanadium dissolution causes the generation and diffusion of vacancies in the oxide layer of the Ti-6Al-4V alloy [41].

The data were fitted with an equivalent circuit to enable an accurate analysis of the impedance diagrams as represented in Fig. 10. In the case of the non-anodized Ti-6Al-4V and Ti-6Al-7Nb alloys, the equivalent circuit is

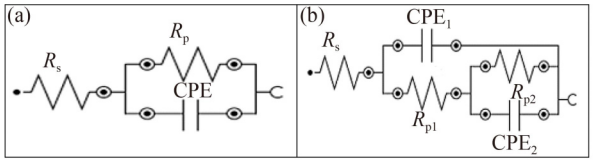

Fig. 10 Equivalent circuits employed for modeling of experimental EIS data (a) with one time constant and (b) with two-time constants.

the simple Randel's circuit (Fig. 10(a)). This circuit involves a constant phase element (CPE) in series with the solution resistance R_s, and parallel to the polarization resistance (charge transfer resistance) of the alloy surface R_p. For the anodized electrode, the equivalent circuit fitted was two-time constants suggesting the formation of two layers (Fig. 10(b)), with solution resistance represented as R_s, double layer capacitance of the outer passive layer of the oxide film represented as CPE_1, and CPE_2 associated with the inner passive layer of the oxide. The charge transfer resistances of the outer layer of the metal/electrolyte interface are represented as R_1 and those of the inner layer as R_2. The passive oxide films on Ti-based alloys are made of two superimposed oxide layers. The first outer passive oxide layer on the top surface is porous, and the second inner passive oxide layer displays a dense barrier-like structure.

The action of the capacitor is compensated by the CPE due to the surface heterogeneity of the surface and is defined by its impedance value:

$$Z_{CPE} = [C(j\omega)^{\alpha}]^{-1}, \quad (8)$$

where α is a surface heterogeneity exponent, $0 \leqslant \alpha \leqslant 1$, j is an imaginary number ($j = (-1)^{1/2}$), $\omega = 2\pi f$ is the angular frequency in rad·s^{-1}, and f is the frequency in Hz = s^{-1} [47]. The outcomes of the EIS analysis are represented in Table 5.

Equation (9) calculates the PE of anodized Ti-6Al-7Nb and Ti-6Al-4V alloys in SBF solution:

$$PE = 1 - \frac{R_p^{\circ}}{R_p} \times 100\%, \quad (9)$$

Table 5 Parameters of electrochemical impedance

	Specimen	R_s/Ω	R_1/kΩ	CPE_1/μF	α_1	R_2/kΩ	CPE_2/μF	α_2	PE/%
Ti-6Al-7Nb	0 V	76	6.20	139.0	0.85	–	–	–	–
	20 V	42	0.34	18.6	0.82	72	403	0.76	91.4
	40 V	45	0.38	15.6	0.83	142	220	0.75	95.5
	60 V	48	0.39	4.9	0.81	63	391	0.78	90.2
	80 V	52	0.43	3.3	0.84	51	430	0.77	88.0
Ti-6Al-4V	0 V	66	4.20	198.0	0.89	–	–	–	–
	20 V	39	0.22	13.6	0.85	40	332	0.75	89.6
	40 V	35	0.23	8.9	0.83	84	90	0.78	95.0
	60 V	46	0.24	3.6	0.84	24	342	0.77	82.7
	80 V	72	0.27	2.7	0.86	18	385	0.76	77.0

where R_p° is the resistances for the titanium alloys before anodization and R_p is the resistances for the titanium alloys after anodization.

Finally, it is worth mentioning that roughness is an important factor controlling implant osseointegration, as there is a relation between surface roughness and cell behavior. A rougher surface increases bone-to-implant contact and maximizes the response of bone cells during tissue healing around dental implants, allowing better osteogenic cell adhesion [48]. Accordingly, in our study, roughening titanium surface through anodization technique provided the required rough oxide surface, as revealed by the AFM results. In a meta-analysis conducted in 2016, it was revealed that anodized surfaces delivered a low implant failure probability [49], additionally; another study proved that anodized titanium surfaces significantly increased blood clot retention and thus favored osseointegration better than non-anodized titanium surfaces [50].

Therefore, according to the work mentioned and within the limitation of the study, anodizing titanium alloys in 10% oxalic acid represented a quick, simple, and inexpensive strategy to improve bone-implant interface and osseointegration. Moreover, the best corrosion performance was acquired by anodizing Ti-6Al-7Nb alloy, which can be suggested for biomedical applications. However, further investigations are required to inspect the bioactivity and osseointegration potential of the proposed anodized alloys on experimental animals *in vivo*.

4 Conclusions

Based on the findings of this study, it was concluded that anodization of Ti-6Al-7Nb and Ti-6Al-4V alloys in 10% oxalic acid solution for 30 s at 20–80 V could successfully produce protective, corrosion resistant, TiO_2 oxide films with different colors, surface morphologies, and a roughness according to the anodization voltage utilized and that the optimal anodization voltage for both alloys is 40 V, with more stable oxide film and superior corrosion resistance for Ti-6Al-7Nb alloy, suggesting its use in the biomedical field.

Competing Interests The authors declare that they have no competing interests.

Electronic Supplementary Material Supplementary material is available in the online version of this article at https://doi.org/10.1007/s11705-023-2368-y and is accessible for authorized users.

Funding note Open access funding provided by The Science, Technology & Innovation Funding Authority (STDF) in cooperation with The Egyptian Knowledge Bank (EKB)

References

1. Resende P D, Junqueira R M R, Silva J D, Lopes N I A, Santos L A, Buono V T L. Comparative study of nanostructured titania grown by electrochemical anodization of α-Ti and β-TiNi substrates in organic electrolytes. Journal of Materials Research and Technology, 2020, 9(5): 10121–10129
2. Sidambe A T. Biocompatibility of advanced manufactured titanium implants: a review. Materials, 2014, 7(12): 8168–8188
3. Peters M, Kumpfert J, Ward C H, Leyens C. Titanium alloys for aerospace applications. Advanced Engineering Materials, 2003, 5(6): 419–427
4. Manjaiah M, Laubscher R F. Effect of anodizing on surface integrity of grade 4 titanium for biomedical applications. Surface and Coatings Technology, 2017, 310: 263–272
5. Placko H E, Mishra S, Weimer J J, Lucas L C. Surface characterization of titanium-based implant materials. International Journal of Oral & Maxillofacial Implants, 2000, 15(3): 355–363
6. Gao A, Hang R, Bai L, Tang B, Chu P K. Electrochemical surface engineering of titanium-based alloys for biomedical application. Electrochimica Acta, 2018, 271: 699–718

7. Suresh K, Geetha M, Richard C, Landoulsi J, Ramasawmy H, Suwas S, Asokamani R. Effect of equal channel angular extrusion on wear and corrosion behavior of the orthopedic Ti-13Nb-13Zr alloy in simulated body fluid. Materials Science and Engineering C, 2012, 32(4): 763–771
8. Nag S, Banerjee R, Fraser H. Microstructural evolution and strengthening mechanisms in Ti-Nb-Zr-Ta, Ti-Mo-Zr-Fe and Ti-15Mo biocompatible alloys. Materials Science and Engineering C, 2005, 25(3): 357–362
9. Durdu S, Sancak M, Yalcin E, Usta M, Akagunduz E, Altinkok A. Surface characterization of TiO_2 nanotube arrays produced on Ti-6Al-4V alloy by anodic oxidation. Surface and Coatings Technology, 2021, 428: 127903–127915
10. Choubey A, Balasubramaniam R, Basu B. Effect of replacement of V by Nb and Fe on the electrochemical and corrosion behavior of Ti-6Al-4V in simulated physiological environment. Journal of Alloys and Compounds, 2004, 381(1-2): 288–294
11. El-Hadad S, Ghaith M, Yassin A, Kamal M, Khalifa W. Optimizing the surface treatment processes to enhance the bioactivity of Ti-6Al-7Nb alloy. Transactions of the Indian Institute of Metals, 2020, 73(11): 2727–2738
12. Prando D, Brenna A, Diamanti M V, Beretta S, Bolzoni F, Ormellese M, Pedeferri M. Corrosion of titanium. Part 2: effects of surface treatments. Journal of Applied Biomaterials & Functional Materials, 2018, 16(1): 3–13
13. Allal N, Bourahla A, Benharcha F, Abdi A, Sayah Z B D, Trari M. Anodizing parameters optimization of Ti-6Al-4V titanium alloy using response surface methodology. Journal of the Indian Chemical Society, 2022, 99(6): 100470–100484
14. Pedeferri M. Titanium anodic oxidation: a powerful technique for tailoring surfaces properties for biomedical applications. In: TMS 2015 144th Annual Meeting & Exhibition (Supplemental Proceedings), 2016. Berlin: Springer, 2016, 515–520
15. Diamanti M V, Del Curto B, Pedeferri M. Anodic oxidation of titanium: from technical aspects to biomedical applications. Journal of Applied Biomaterials & Biomechanics: JABB, 2011, 9(1): 55–69
16. Hall D J, Urban R M, Pourzal R, Turner T M, Skipor A K, Jacobs J J. Nanoscale surface modification by anodic oxidation increased bone ingrowth and reduced fibrous tissue in the porous coating of titanium-alloy femoral hip arthroplasty implants. Journal of Biomedical Materials Research. Part B, Applied Biomaterials, 2017, 105(2): 283–290
17. Bandeira R M, Rêgo G C, Picone C A, van Drunen J, Correr W R, Casteletti L C, Machado S A S, Tremiliosi-Filho G. Alternating current oxidation of Ti-6Al-4V alloy in oxalic acid for corrosion resistant surface finishing. SN Applied Sciences, 2020, 2(6): 1092
18. Pilipenko A, Maizelis A, Pancheva H, Zhelavskaya Y A. Electrochemical oxidation of VT6 titanium alloy in oxalic acid solutions. Chemistry & Chemical Technology, 2020, 14(2): 221–226
19. Sul Y T, Johansson C B, Jeong Y, Albrektsson T. The electrochemical oxide growth behaviour on titanium in acid and alkaline electrolytes. Medical Engineering & Physics, 2001, 23(5): 329–346
20. Sul Y T, Byon E, Wennerberg A. Surface characteristics of electrochemically oxidized implants and acid-etched implants: surface chemistry, morphology, pore configurations, oxide thickness, crystal structure, and roughness. International Journal of Oral & Maxillofacial Implants, 2008, 23(4): 631–640
21. Keshavarz A, Parang Z, Nasseri A. The effect of sulfuric acid, oxalic acid, and their combination on the size and regularity of the porous alumina by anodization. Journal of Nanostructure in Chemistry, 2013, 3(1): 34–38
22. Liu L M, Crawford P, Hu P. The interaction between adsorbed OH and O_2 on TiO_2 surfaces. Progress in Surface Science, 2009, 84(5-6): 155–176
23. Standard A. E112: standard test methods for determining average grain size. West Conshocken, 1996, 112: 4–20
24. Abdel-Gawad S A, Shoeib M A. Corrosion studies and microstructure of Mg-Zn-Ca alloys for biomedical applications. Surfaces and Interfaces, 2019, 14: 108–116
25. Shoeib M A, Abdel-Gawad S A. High performance nano hydroxyapatite coating on zinc for biomedical applications. Journal of Materials Science, 2023, 58(2): 740–756
26. Abdel-Salam M, El-Hadad S, Khalifa W. Effects of microstructure and alloy composition on hydroxyapatite precipitation on alkaline treated α/β titanium alloys. Materials Science and Engineering C, 2019, 104: 109974–109985
27. Zaki A, El-Hadad S, Khalifa W. Surface modification effects on microstructure and mechanical properties of bio-titanium alloys. Materials Science Forum, 2017, 909: 199–204
28. Liu X, Wu S, Yeung K W, Chung C Y, Chu P K. Surface Coloration and electrochemical impedance spectroscopy characterization of oxygen plasma implanted orthopaedic titanium alloys. International Journal of Electrochemical Science, 2012, 7(8): 6638–6653
29. Holmberg R J, Beauchemin D, Jerkiewicz G. Characteristics of colored passive layers on titanium: morphology, optical properties, and corrosion resistance. ACS Applied Materials & Interfaces, 2014, 6(23): 21576–21584
30. Kumar A, Kushwaha M K. Tribological behavior of nanoporous anodic film obtained on titanium grade-5 alloy. Advanced Science, Engineering and Medicine, 2019, 11(6): 565–570
31. Garsivaz jazi M, Golozar M, Raeissi K, Fazel M. Surface characteristics and electrochemical impedance investigation of spark-anodized Ti-6Al-4V alloy. Journal of Materials Engineering and Performance, 2014, 23(4): 1270–1278
32. Hosseini M G, Momeni M, Faraji M. Highly active nickel nanoparticles supported on TiO_2 nanotube electrodes for methanol electrooxidation. Electroanalysis, 2010, 22(22): 2620–2625
33. Wang T, Wang L, Lu Q, Fan Z. Changes in the esthetic, physical, and biological properties of a titanium alloy abutment treated by anodic oxidation. Journal of Prosthetic Dentistry, 2019, 121(1): 156–165
34. Park K, Heo S, Koak J, Kim S, Lee J, Kim S, Lim Y. Osseointegration of anodized titanium implants under different current voltages: a rabbit study. Journal of Oral Rehabilitation, 2007, 34(7): 517–527
35. b Achoi M F, bt Asiah M N, Rusop M, Abdullah S. The effect of

growth temperature on the surface properties of TiO_2 nanostructures grown on TiO_2 templates. Transactions of the Materials Research Society of Japan, 2011, 36(2): 273–279

36. Melo-Fonseca F, Gasik M, Madeira S, Silva F, Miranda G. Surface characterization of titanium-based substrates for orthopaedic applications. Materials Characterization, 2021, 177: 111161–111175
37. Mazzarolo A, Curioni M, Vicenzo A, Skeldon P, Thompson G. Anodic growth of titanium oxide: electrochemical behaviour and morphological evolution. Electrochimica Acta, 2012, 75: 288–295
38. Shabalovskaya S, Anderegg J, Van Humbeeck J. Critical overview of nitinol surfaces and their modifications for medical applications. Acta Biomaterialia, 2008, 4(3): 447–467
39. Saraswati W C, Anawati A, Jujur I N, Gumelar M D. Effect of coloring by anodizing on the corrosion behavior of Ti-6Al-4V alloy. AIP Conference Proceedings, AIP Publishing 2020, 2232(1): 020004–020008
40. Han M K, Kim J Y, Hwang M J, Song H J, Park Y J. Effect of Nb on the microstructure, mechanical properties, corrosion behavior, and cytotoxicity of Ti-Nb alloys. Materials, 2015, 8(9): 5986–6003
41. Metikoš-Huković M, Kwokal A, Piljac J. The influence of niobium and vanadium on passivity of titanium-based implants in physiological solution. Biomaterials, 2003, 24(21): 3765–3775
42. Tamilselvi S, Raman V, Rajendran N. Corrosion behaviour of Ti-6Al-7Nb and Ti-6Al-4V ELI alloys in the simulated body fluid solution by electrochemical impedance spectroscopy. Electrochimica Acta, 2006, 52(3): 839–846
43. Al-Mobarak N, Al-Swayih A, Al-Rashoud F. Corrosion behavior of Ti-6Al-7Nb alloy in biological solution for dentistry applications. International Journal of Electrochemical Science, 2011, 6(6): 2031–2042
44. Shaw B, Stephen D. ASM Handbook Volume 13A: Corrosion: Fundamentals. Testing and Protection. Materials Park (Ohio, USA): ASM International, 2003
45. Hammam R E, Abdel-Gawad S A, Moussa M E, Shoeib M, El-Hadad S. Study of microstructure and corrosion behavior of cast Zn-Al-Mg alloys. International Journal of Metalcasting, 2023
46. Francis A, Abdel-Gawad S A, Shoeib M. Toward CNT-reinforced chitosan-based ceramic composite coatings on biodegradable magnesium for surgical implants. Journal of Coatings Technology and Research, 2021, 18(4): 971–988
47. Medany S S, Elkamel R S, Abdel-Gawad S A, Fekry A M. A novel nano-composite CSNPs/PVP/CoONPs coating for improving corrosion resistance of Ti-6Al-4V alloy as a dental implant. Metals, 2022, 12(11): 1784–1796
48. Matos G R M. Surface roughness of dental implant and osseointegration. Journal of Maxillofacial and Oral Surgery, 2021, 20(1): 1–4
49. Chrcanovic B, Albrektsson T, Wennerberg A. Turned versus anodised dental implants: a meta-analysis. Journal of Oral Rehabilitation, 2016, 43(9): 716–728
50. Traini T, Murmura G, Sinjari B, Perfetti G, Scarano A, D'Arcangelo C, Caputi S. The surface anodization of titanium dental implants improves blood clot formation followed by osseointegration. Coatings, 2018, 8(7): 252–265